Crystal Structure and Physical Properties of New Ternary Gallides $Eu_2Rh_3Ga_9$ and $Eu_2Ir_3Ga_9$

Olga Sichevych[a,b], Walter Schnelle[a], Yurii Prots[a], Ulrich Burkhardt[a], and Yurii Grin[a]

[a] Max-Planck-Institut für Chemische Physik fester Stoffe, Nöthnitzer Straße 40, 01187 Dresden, Germany
[b] Institute of Chemistry, Ukrainian State Forestry Academy, General Chuprinky Street 105, 79013 Lviv, Ukraine

Reprint requests to Yu. Grin. E-mail: grin@cpfs.mpg.de

Z. Naturforsch. **61b,** 904 – 911 (2006); received March 17, 2006

Dedicated to Professor Wolfgang Jeitschko on the occasion of his 70th birthday

The compounds $Eu_2Rh_3Ga_9$ and $Eu_2Ir_3Ga_9$ were synthesized by melting the elements in sealed tantalum tubes with subsequent annealing at 600 °C. Both gallides are isotypic with $Y_2Co_3Ga_9$ (space group *Cmcm*, Pearson symbol *oC*56, $Z = 4$) as evidenced by single crystal structure analysis: $a = 12.9902(6)$, $b = 7.6141(4)$, $c = 9.7433(5)$ Å, $R_F = 0.025$, 617 structure factors, 42 variable parameters for $Eu_2Rh_3Ga_9$, and $a = 13.0371(7)$, $b = 7.6017(4)$, $c = 9.6972(6)$ Å, $R_F = 0.032$, 645 reflections, 42 variables for $Eu_2Ir_3Ga_9$. Magnetic susceptibility measurements as well as X-ray absorption spectra indicate the $4f^7$ electronic configuration of europium (Eu^{2+}) with significant admixture of the $4f^6$ state in both compounds.

Key words: Europium, Gallium, Intermetallic Compounds, Magnetic Properties, X-Ray Absorption Spectra

Introduction

Recent investigations of aluminium- and gallium-rich phases of rare-earths (*RE*) with transition metals (*T*) revealed several series of ternary compounds exhibiting similar building principles to those found initially in the structure of $Y_2Co_3Ga_9$ [1]: alternation of nearly planar and slightly puckered layers with pseudo-trigonal symmetry and RE_2M_3 and TM_2 compositions, respectively (M = Al or Ga). Different stacking of these slabs (sometimes in combination with additional kinds of layers) results in very similar compositions and quite a variety of symmetries: $Yb_2Pd_3Ga_9$ (space group $P6_122$, Pearson symbol *hP*84) [2], $RENi_3Al_9$ (*RE* = Y, Gd, Dy, Er; space group *R*32, Pearson symbol *hR*78) [3], $RE_4\underline{T}_9Al_{24}$ (*RE* = Y, Gd–Lu; T = Pd, Pt; space group *P*1, Pearson symbol *aP*37) [4], $RE_{2-x}Pt_4M_{8+3x}$ (*RE* = Y, La–Sm, Gd, Er, Yb; space group $P6_3/mmc$, Pearson symbol *hP*20 – 4.3) [5 – 7]. Representatives of the $Y_2Co_3Ga_9$ structure type (space group *Cmcm*, Pearson symbol *oC*56) are reported mainly for ternary rare-earth aluminides (gallides) containing Co, Rh, Ir, Ru and Pd as transition element: $RE_2Co_3Ga_9$ (*RE* = Y, Gd–Lu) [1, 8 – 10], $RE_2Co_3Al_9$ (*RE* = Y, Yb, Lu) [9 – 11], $RE_2Rh_3Ga_9$ (*RE* = Y, Ce, Sm, Gd–Yb) [12 – 16], $RE_2Rh_3Al_9$ (*RE* = Y, La–Sm, Gd–Lu) [13, 14, 16 – 18], $RE_2Ir_3Ga_9$ (*RE* = Y, Ce, Sm, Gd–Yb) [12 – 16], $RE_2Ir_3Al_9$ (*RE* = Y, La–Sm, Gd–Lu) [13, 14, 17 – 19], $RE_2Ru_3Ga_9$ (*RE* = Y, La–Sm, Gd–Tm) [20 – 22] and $RE_2Pd_3Al_9$ (*RE* = Y, Gd–Tm) [17]. Ternary phases $Sc_2Co_3Ga_9$, $Sc_2Co_3Al_9$, $Zr_2Co_3Al_9$ and $Hf_2Co_3Al_9$ [23] also should be mentioned as isotypic. Increased interest in the cerium and ytterbium as well as in the uranium compounds ($U_2Ir_3Al_9$ [18], $U_2T_3M_9$, T = Rh, Ir, M = Al, Ga [13]) is motivated by various magnetic, electrical and transport properties, like intermediate valence, a variety of magnetic ordering phenomena, strong Kondo interactions *etc*. Similar peculiarities can be expected for respective europium compounds. However, no $Eu_2T_3M_9$ phase was synthesized until recently. Subject of the present study are the gallides $Eu_2Rh_3Ga_9$ and $Eu_2Ir_3Ga_9$, the first europium containing representatives of the $Y_2Co_3Ga_9$ structure type.

Experimental Section

Starting materials for the preparation of $Eu_2Rh_3Ga_9$ and $Eu_2Ir_3Ga_9$ were ingots of europium (Johnson Matthey, stated

purity 99.9%), rhodium foil (ChemPur, 99.9%), iridium foil (Lamprecht, 99.9%), and gallium lumps (ChemPur, 99.99%), respectively. To minimize ferromagnetic impurities like EuO or EuN, europium was redistilled in vacuum before use. The pieces of the elemental components were mixed in stoichiometric ratios and sealed into tantalum tubes under an argon pressure of about 800 mbar. The tantalum tubes were subsequently enclosed into evacuated silica ampoules to prevent oxidation of tantalum during the high temperature treatment. In the first step of the synthesis, the ampoules were heated to 900 °C within 24 h and held at this temperature for 2 d. After that, the temperature was slowly (50 °C/d) lowered to 600 °C. The samples were annealed at this temperature for 2 weeks and subsequently quenched in cold water. Alternatively, both compounds can be obtained by high-frequency melting of the elemental components in an open glassy carbon crucible under argon atmosphere with a subsequent annealing under the same conditions (600 °C, 2 weeks). Both synthetic routes lead to single phase products as can be concluded from X-ray powder diffraction and microstructure analysis. To prevent reaction of the starting materials and products with air and moisture, all manipulations were performed inside an argon-filled glove box ($p(O_2/H_2O) \leq 0.1$ ppm, purification by molecular sieve and copper catalyst). The gallides obtained in bulk form are quite stable against air, however, the powdered samples are oxidized within a few days.

The samples were characterized by X-ray powder diffraction using an Imaging Plate Guinier Camera (HUBER G670 Co-$K_{\alpha 1}$ radiation, $\lambda = 1.788965$ Å, 6×15 min scans, measured range $6^\circ \leq 2\theta \leq 100^\circ$). Unit cell parameters were refined by a least squares procedure using the peak positions extracted from powder patterns measured with LaB_6 as internal standard ($a = 4.15692$ Å). Indexing of the diffraction peaks in the powder diagrams was controlled by intensity calculations using positional parameters of the refined structures. All crystallographic calculations were performed with the Windows version of the program package CSD (WinCSD) [24].

Irregularly shaped crystals of $Eu_2Rh_3Ga_9$ and $Eu_2Ir_3Ga_9$ were isolated from the annealed samples and their quality was checked by Laue photographs. The intensity data sets were collected from the qualitatively best single crystals on a STOE IPDS setup (graphite monochromator, Ag-K_α radiation, $\lambda = 0.56087$ Å) by oscillation of the crystals around the φ axis. The numerical absorption corrections were performed on the basis of the optimized description of the crystal faces [25]. The starting atomic parameters were obtained from direct methods. The crystal structures were successfully refined with anisotropic displacement parameters for all atoms. For interatomic distances calculations, lattice parameters obtained from Guinier powder diffraction data were used in the last runs of the refinement. Whole relevant crystallographic information and details for the data collection and handling are listed in Table 1. Atomic parameters and selected interatomic distances are given in Tables 2 and 3.*

Table 1. Crystallographic data for $Eu_2Rh_3Ga_9$ and $Eu_2Ir_3Ga_9$ (space group *Cmcm*, *oC*56, $Z = 4$).

Composition	$Eu_2Rh_3Ga_9$	$Eu_2Ir_3Ga_9$
Unit cell parameters		
a [Å]	12.9902(6)	13.0371(7)
b [Å]	7.6141(4)	7.6017(4)
c [Å]	9.7433(5)	9.6972(6)
V [Å^3]	963.7(1)	961.0(2)
Calc. density [g/cm]	8.55	10.42
Crystal size [μm^3]	$25 \times 45 \times 70$	$35 \times 45 \times 80$
Absorption coeff. [mm^{-1}]	22.8	44.0
Diffraction system	STOE IPDS	STOE IPDS
Radiation, λ [Å]	Ag, 0.56087	Ag, 0.56087
Scans, step	φ, 0.8	φ, 0.8
N(images)	225	250
2θ up to [°]	47.8	47.6
Range in h,k,l	± 18, ± 10, ± 14	± 18, ± 10, ± 13
Absorption correction	numerical	numerical
$T(\max)/T(\min)$	1.67	1.95
$N(hkl)$ measuared	5591	6090
$N(hkl)$ unique	830	816
R(int)	0.059	0.049
$N(hkl)$ observed	617	645
Observation criteria	$F(hkl) > 4\sigma(F)$	$F(hkl) > 4\sigma(F)$
Refined parameters	42	42
Extinction parameter	0.00044(3)	0.00002(1)
$R(F)$	0.025	0.032
Residual peak [e/Å^3]	1.67	2.07

Microstructure analysis was performed on the annealed samples by using light optical microscopy (Zeiss Axioplan 2) as well as scanning electron microscopy (SEM, Philipps XL 30). The polished ingots were prepared under inert conditions in an argon filled glove-box. Silicon carbide (SiC) paper was used for grinding, and diamond polishing with at least $1/4$ μm diamond powder was applied for finishing. The microstructure surface was cleaned in a hexane bath from the paraffin oil which acts as lubricant for the preparation of microstructures.

The standard-less energy dispersive X-ray absorption analysis (EDXS) was performed on an EDAX system attached to the Philipps XL 30 SEM with LaB_6 cathode. The spectra, recorded at 25 kV by the Si(Li)-drift detector, showed solely the presence of the constituent elements of the respective ternary compounds.

The magnetization of the polycrystalline samples was measured in a SQUID magnetometer (MPMS XL-7, Quantum Design) between 1.8 and 400 K in magnetic fields be-

*Further details on the crystal structure investigations can be obtained from the Fachinformationzentrum Karlsruhe, D-76344 Eggenstein-Leopoldshafen, Germany, fax: (+49)7247-808-666; e-mail: crysdata@fiz.karlsruhe.de, on quoting the depository numbers CSD 416379 ($Eu_2Rh_3Ga_9$) and CSD 416378 ($Eu_2Ir_3Ga_9$).

Table 2. Atomic coordinates and displacement parameters (in Å^2) for $Eu_2Rh_3Ga_9$ and $Eu_2Ir_3Ga_9$.

Atom	Site	x	y	z	B_{11}	B_{22}	B_{33}	B_{12}	B_{13}	B_{23}	B_{eq}*
					$Eu_2Rh_3Ga_9$						
Eu	8*g*	0.16338(5)	0.16597(8)	3/4	0.43(2)	0.31(2)	0.33(2)	0.02(2)	0	0	0.36(1)
Rh1	4*a*	0	0	1/2	0.30(4)	0.20(4)	0.43(5)	0	0	0.10(4)	0.31(3)
Rh2	8*e*	0.32876(8)	0	1/2	0.26(3)	0.25(3)	0.31(3)	0	0	−0.09(3)	0.28(2)
Ga1	8*f*	1/2	0.1639(2)	0.4441(2)	0.37(4)	0.36(4)	0.92(5)	0	0	−0.02(4)	0.55(3)
Ga2	16*h*	0.16544(7)	0.1704(1)	0.4269(1)	0.44(3)	0.34(3)	0.58(3)	−0.02(3)	−0.08(3)	−0.01(3)	0.45(2)
Ga3	4*c*	0	0.1306(3)	1/4	0.67(7)	0.56(7)	0.40(6)	0	0	0	0.54(4)
Ga4	8*g*	0.3955(1)	0.0587(2)	3/4	0.60(5)	0.60(5)	0.38(4)	−0.00(4)	0	0	0.52(3)
					$Eu_2Ir_3Ga_9$						
Eu	8*g*	0.16371(9)	0.1670(1)	3/4	0.34(3)	0.36(3)	0.32(4)	0.07(3)	0	0	0.34(2)
Ir1	4*a*	0	0	1/2	0.25(4)	0.33(4)	0.24(4)	0	0	0.10(3)	0.28(2)
Ir2	8*e*	0.32929(6)	0	1/2	0.20(2)	0.33(3)	0.23(3)	0	0	−0.04(2)	0.25(1)
Ga1	8*f*	1/2	0.1649(3)	0.4436(3)	0.27(7)	0.52(8)	0.97(10)	0	0	−0.13(8)	0.59(5)
Ga2	16*h*	0.1661(1)	0.1684(3)	0.4266(2)	0.36(5)	0.46(5)	0.55(6)	−0.04(5)	−0.10(5)	0.04(5)	0.46(3)
Ga3	4*c*	0	0.1303(5)	1/4	0.87(12)	0.27(12)	0.20(11)	0	0	0	0.45(7)
Ga4	8*g*	0.3964(2)	0.0598(3)	3/4	0.27(8)	0.69(8)	0.34(8)	−0.02(7)	0	0	0.47(5)

* $B_{eq} = 1/3[B_{11}a^{*2}a^2 + \ldots 2B_{23}b^*c^*bc\cos\alpha]$.

Table 3. Selected interatomic distances (in Å) in the gallides $Eu_2Rh_3Ga_9$ and $Eu_2Ir_3Ga_9$.

Atoms*	$Eu_2Rh_3Ga_9$	$Eu_2Ir_3Ga_9$	Atoms		$Eu_2Rh_3Ga_9$	$Eu_2Ir_3Ga_9$	Atoms		$Eu_2Rh_3Ga_9$	$Eu_2Ir_3Ga_9$
Eu –2Ga2	3.077(1)	3.069(2)	Ga1 –	2*T*2	2.608(1)	2.612(2)	Ga4 –	2*T*2	2.6236(8)	2.617(1)
2Ga2	3.086(1)	3.070(2)		1*T*1	2.616(2)	2.606(3)		1Ga4	2.715(2)	2.706(4)
1Ga4	3.087(2)	3.086(3)		1Ga1	2.723(2)	2.735(4)		1Ga3	2.727(2)	2.716(4)
1Ga3	3.098(2)	3.110(3)		2Ga2	2.791(2)	2.808(3)		2Ga2	2.802(2)	2.804(3)
1Ga4	3.123(2)	3.139(3)		2Ga4	2.879(2)	2.875(3)		2Ga1	2.879(2)	2.875(3)
2Ga1	3.123(1)	3.117(2)		2Eu	3.123(1)	3.117(2)		1Eu	3.087(2)	3.086(3)
2Ga2	3.148(1)	3.138(2)	Ga2 –	1*T*2	2.586(1)	2.583(2)		1Eu	3.123(2)	3.139(3)
2*T*1	3.4687(8)	3.471(1)		1*T*1	2.609(1)	2.614(2)				
2*T*2	3.485(1)	3.485(1)		1*T*2	2.610(1)	2.621(2)				
2*T*2	3.5229(7)	3.5062(7)		1Ga3	2.771(1)	2.775(2)				
1Eu	4.244(1)	4.270(2)		1Ga1	2.791(2)	2.808(3)				
2Eu	4.422(1)	4.416(2)		1Ga4	2.802(2)	2.804(3)				
*T*1 –4Ga2	2.609(1)	2.614(2)		1Ga2	2.886(2)	2.893(3)				
2Ga1	2.616(2)	2.606(3)		1Ga2	2.960(1)	2.930(3)				
2Ga3	2.6307(9)	2.619(1)		1Eu	3.077(1)	3.069(2)				
4Eu	3.4687(8)	3.471(1)		1Eu	3.086(1)	3.070(2)				
*T*2 –2Ga2	2.586(1)	2.583(2)		1Eu	3.148(1)	3.138(2)				
2Ga1	2.608(1)	2.612(2)	Ga3 –	2*T*1	2.6307(9)	2.619(1)				
2Ga2	2.610(1)	2.621(2)		2Ga4	2.727(2)	2.716(4)				
2Ga4	2.6236(8)	2.617(1)		4Ga2	2.771(1)	2.775(2)				
2Eu	3.485(1)	3.485(1)		2Eu	3.098(2)	3.110(3)				
2Eu	3.5229(7)	3.5062(7)								

$T \equiv$ Rh or Ir.

tween 100 Oe and 70 kOe. Electrical resistivity was measured on roughly bar-shaped pieces by a conventional dc four-point method. The inaccuracy due to the geometry is ±40%.

The Eu-L_{III} X-ray absorption spectra (XAS) of polycrystalline $Eu_2Rh_3Ga_9$ and $Eu_2Ir_3Ga_9$ were recorded in transmission arrangement at the EXAFS II beamline A1 of HASYLAB at DESY. Wavelength selection was realized by means of a Si(111) double crystal monochromator which yields an experimental resolution of approximately 2 eV (FWHM) for the experimental setup at the Eu-L_{III} threshold of 6977 eV. Experimental data were measured using Eu_2O_3 as an external reference compound for energy calibration. Deconvolution of the XAS spectra was performed with the program XasWin [26].

Results and Discussion

Microstructure and composition

The microstructure of the samples with nominal compositions $Eu_{14.3}Rh_{21.4}Ga_{64.3}$ and $Eu_{14.3}Ir_{21.4}$

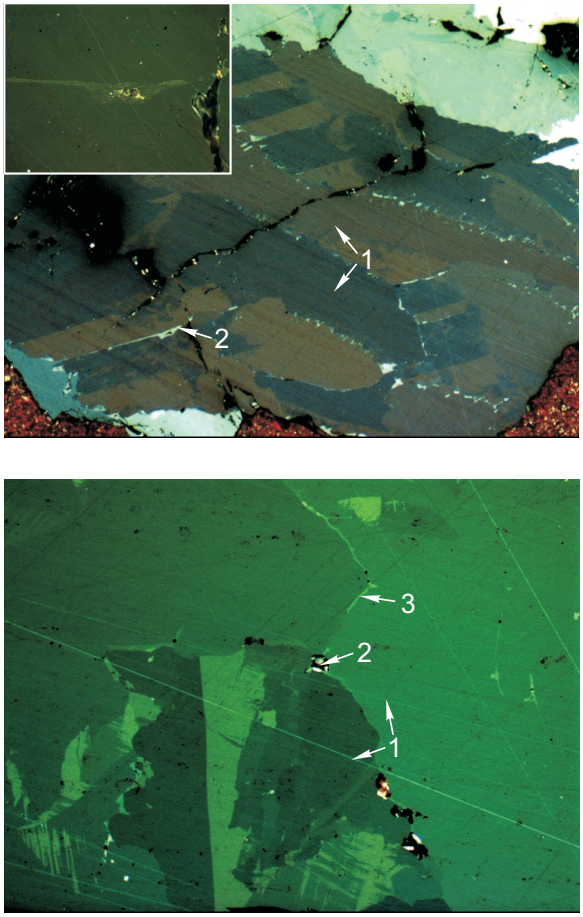

Fig. 1. Microstructure of the samples $Eu_2Rh_3Ga_9$ (top) and $Eu_2Ir_3Ga_9$ (bottom). The polarized light images show differently oriented grains of the main phase (1) together with a small amount of impurities: $EuRh_2Ga_8$ (2), $IrGa_2$ (2) and $IrGa_3$ (3), respectively.

$Ga_{64.3}$ is formed mainly by the target compounds $Eu_2Rh_3Ga_9$ and $Eu_2Ir_3Ga_9$, respectively (Fig. 1). The compositions of the majority phases obtained from the EDXS spectra – $Eu_{14.6(1)}Rh_{20.1(3)}Ga_{65.3(2)}$ and $Eu_{14.5(3)}Ir_{21.5(3)}Ga_{64.0(6)}$[†] – are, especially for the iridium compound, in agreement with the results of the crystal structure determination. Only traces of minority phases were observed on the grain boundaries of the majority phase: $EuRh_2Ga_8$ in the rhodium-containing sample; $IrGa_2$ and $IrGa_3$ in the iridium-containing sample.

[†]Uncertainties (in parentheses) were obtained from 5 measured points for each sample.

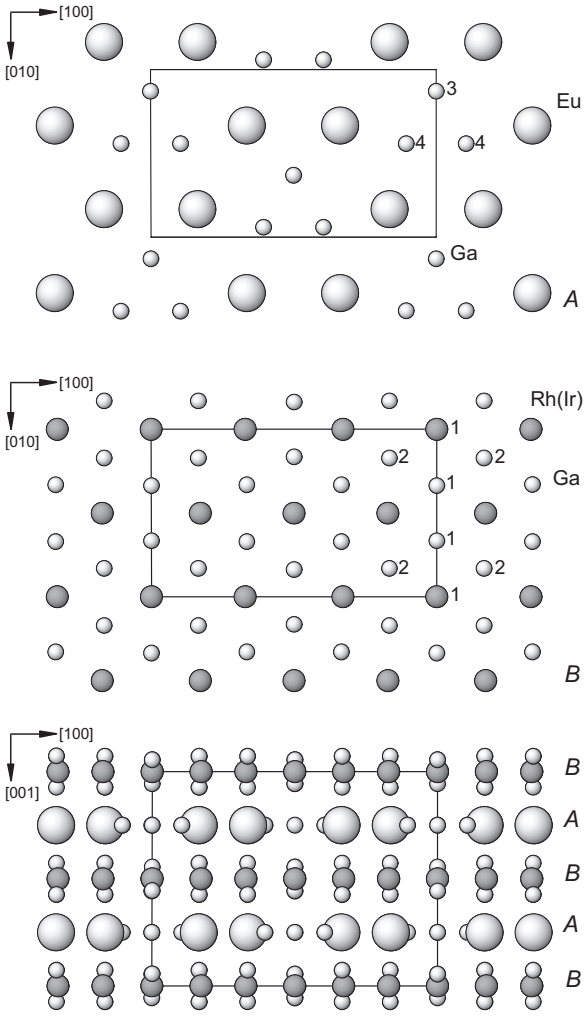

Fig. 2. Flat layers *A* (top), puckered layers *B* (middle) and their stacking in the crystal structures of $Eu_2Rh_3Ga_9$ and $Eu_2Ir_3Ga_9$ (bottom). The numbers close to the circles represent the atom designations of the rhodium (iridium) and gallium atoms, respectively.

Structure chemistry

The orthorhombic crystal structures of the gallides $Eu_2Rh_3Ga_9$ and $Eu_2Ir_3Ga_9$ adopt the $Y_2Co_3Ga_9$ type. Along [001] the crystal structure can be described as a stacking of two types of layers: flat layer *A* and puckered layer *B* with the stacking sequence $\ldots(AB)_2\ldots$. Planar layers of type *A* with the composition Eu_4Ga_6 contain two-dimensional hexagonal close packing-like arrangement of europium atoms, where one third of the atoms has been replaced by triangular Ga_3 clusters. Rhodium (iridium) and gallium atoms of the lay-

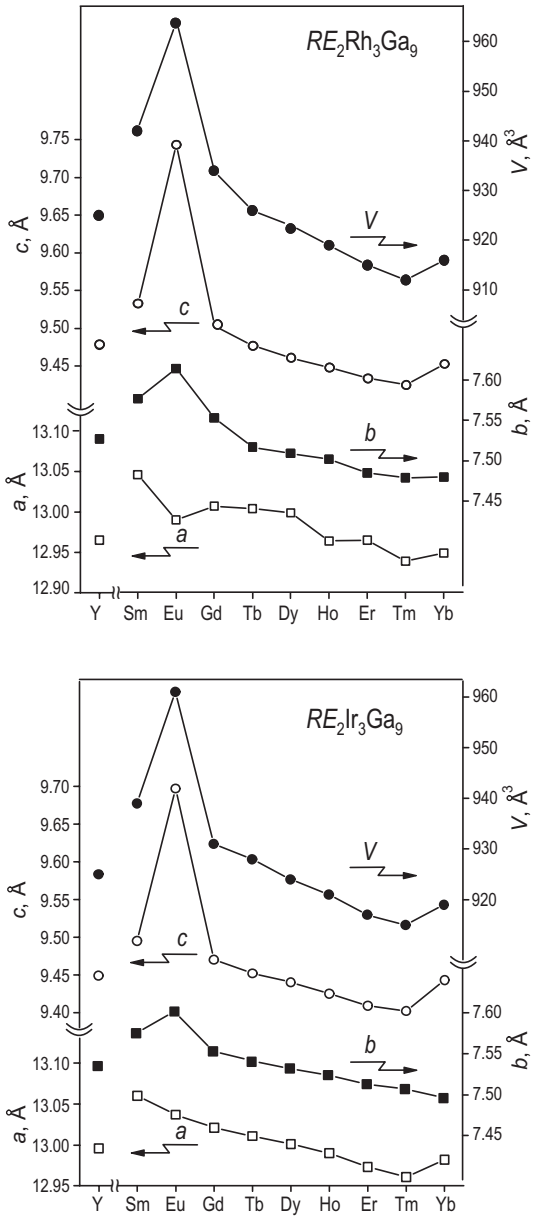

Fig. 3. Lattice parameters and unit cell volumes of compounds $RE_2Rh_3Ga_9$ (top) and $RE_2Ir_3Ga_9$ (bottom). The estimated standard deviations (e. s. d.) in all cases are smaller than the symbols.

ers *B* form strongly puckered hexagonal arrangement, derived from a close packed one, with a T : Ga ratio of 1 : 2 (Rh_6Ga_{12} or Ir_6Ga_{12}, Fig. 2). It is remarkable, that both layers reveal clearly a trigonal symmetry. Nevertheless, on stacking, their 3-fold axes do not coincide. This explains the overall orthorhombic symmetry of both crystal structures with an a/b ratio close to $\sqrt{3}$ (1.706 for $Eu_2Rh_3Ga_9$ and 1.715 for $Eu_2Ir_3Ga_9$).

The compounds $Eu_2Rh_3Ga_9$ and $Eu_2Ir_3Ga_9$ complete the respective series of ternary rhodium (iridium) gallides reported for Y, Ce, Sm, Gd–Yb as rare-earth components [12]. The cell volumes of $RE_2Rh_3Ga_9$ and $RE_2Ir_3Ga_9$ (Fig. 3) deviate significantly from the values expected for the lanthanoid contraction, suggesting a non-trivalent state of europium in these phases. Remarkably, in both series only the *b* and *c* lattice parameters contribute to the increase of the unit cell volumes whereas lattice parameters *a* fit rather well between the respective values of the samarium and gadolinium compounds. To show these contributions quantitatively we compare *b*, *c* and *V* parameters of $Eu_2Rh_3Ga_9$ and $Eu_2Ir_3Ga_9$ with values obtained by averaging the respective lattice constants of the Sm and Gd phases [12] (as should be expected in case of the lanthanoid contraction). These result in the increasing factors $\Delta b = +0.65\%$ and $+0.50\%$, $\Delta c = +2.37\%$ and $+2.26\%$, $\Delta V = +2.74\%$ and $+2.78\%$ for $Eu_2Rh_3Ga_9$ and $Eu_2Ir_3Ga_9$, respectively.

The strongly anisotropic behaviour of the lattice parameters with different *RE* components can be understood from the layered crystal structure (Fig. 2). Let us assume that Rh(Ir) and Ga are covalently bonded in these crystal structures like it was recently shown for the binary compounds $IrGa_2$ [27], Rh_3Ga_{16} and Rh_4Ga_{21} [28]. In this case, the lattice parameters *a* and *b* are controlled by the layer *B* containing only gallium and transition metal atoms with short distances of ≈ 2.60 Å, comparable with the sum of covalent radii of Rh, Ir and Ga (1.25, 1.27 and 1.25 Å, respectively [29]). The *T*–Ga distances between the layers *A* and *B* are longer (up to 2.8 – 2.9 Å), indicating weaker interactions. Thus, the *RE* component may influence

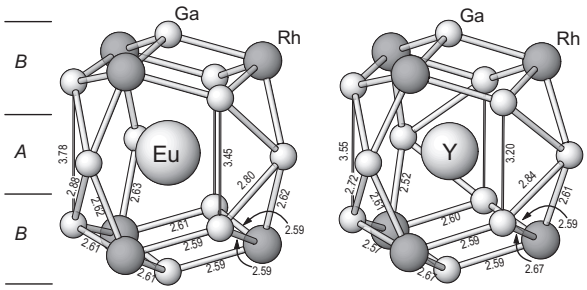

Fig. 4. Selected interatomic distances within the atomic environment of *RE* atoms in the crystal structures of $Eu_2Rh_3Ga_9$ (left) and $Y_2Rh_3Ga_9$ (right).

mainly the lattice parameter *c*, which can be clearly recognized also by comparing the coordination of the *RE* atoms in the crystal structures of $Eu_2Rh_3Ga_9$ and $Y_2Rh_3Ga_9$ [12] (Fig. 4).

Magnetism and electrical resistivity

The inverse magnetic susceptibilities $\chi = M/H$ of the two compounds are plotted in Fig. 5. Except for the lowest temperatures the data are well described by the Curie-Weiss law. The following parameters result from fits of $\chi(T)$: $Eu_2Rh_3Ga_9$, range of fit 50 K to 400 K, paramagnetic effective moment $\mu_{\rm eff} = 7.77\ \mu_{\rm B}$/(atom Eu), $\Theta = -18.9(2)$ K; $Eu_2Ir_3Ga_9$, 50 K to 330 K, $\mu_{\rm eff} = 7.74\ \mu_{\rm B}$/(atom Eu), $\Theta = -23.2(1)$ K. The effective magnetic moments of both compounds indicate the $^8S_{7/2}$ ground multiplet of the $4f^7$ configuration of Eu^{2+}, whereby the values of the effective magnetic moments are somewhat smaller than the expected value of 7.94 $\mu_{\rm B}$ for the $4f^7$ configuration. The negative Θ values hint for predominantly antiferromagnetic interactions. $Eu_2Rh_3Ga_9$ orders antiferromagnetically at $T_{\rm N} = 19.5(7)$ K, as indicated by a small peak in the low-field susceptibility $\chi(T)$ followed by a strong decrease below that temperature (inset of Fig. 5). Since the size of the peak depends on whether the measurement was taken after zero-field cooling or in field cooling, a small ferromagnetic component seems to exist for temperatures just below $T_{\rm N}$. A magnetization isotherm taken at 1.8 K increases linearly to $M/(\text{atoms Eu}) = 0.94\ \mu_{\rm B}$ at 70 kOe and shows no special features in this respect. $Eu_2Ir_3Ga_9$ also orders antiferromagnetically (at $T_{\rm N} = 17.5(5)$ K) with a cusp and a strong decrease of $\chi(T)$ below $T_{\rm N}$. An isotherm at 1.8 K increases linearly to 0.14 $\mu_{\rm B}$/(Eu-atom) at 60 kOe, but above this field there are indications for a metamagnetic transition. At our maximum field of 70 kOe the magnetization per Eu-atom is already 0.22 $\mu_{\rm B}$.

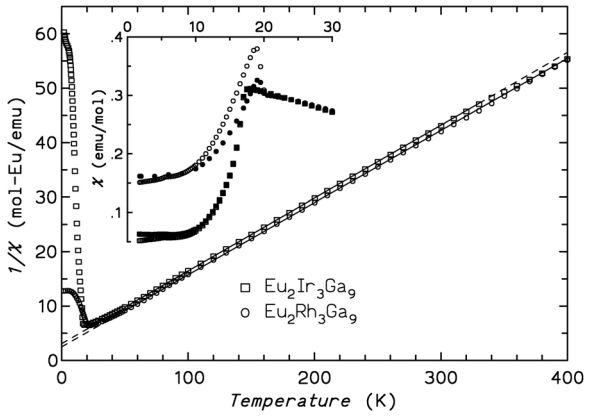

Fig. 5. Inverse magnetic susceptibility $1/\chi$ for $H = 10$ kOe. The full and dashed lines are Curie-Weiss fits to the data above 50 K and the extrapolation to $T = 0$. The inset shows $\chi(T)$ for $H = 100$ Oe measured on warming after zero-field cooling (zfc; open symbols) and during cooling in field (fc; filled symbols).

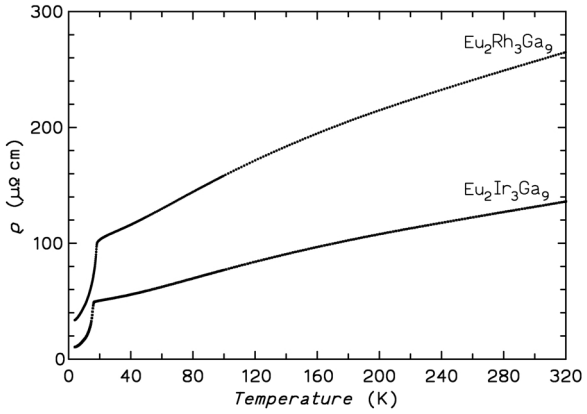

Fig. 6. Temperature dependence of the electrical resistivity for the $Eu_2Rh_3Ga_9$ and $Eu_2Ir_3Ga_9$ samples.

The temperature dependence of the electrical resistivity $\rho(T)$ (Fig. 6) reveals a metal-like conduction behaviour for both materials. The relatively high absolute values of the resistivity are in agreement with the mostly covalent interatomic interactions deduced from the structural features. The kinks in the resistivity around 20 K reflect antiferromagnetic ordering, the temperatures of these features being in agreement with the measurements of magnetic susceptibility. A strong reduction of $\rho(T)$ below $T_{\rm N}$ is expected for Eu^{2+} compounds due to the large deGennes factor (which is maximum among the *RE* ions).

X-ray absorption spectroscopy

The X-ray absorption spectra of $Eu_2Rh_3Ga_9$ and $Eu_2Ir_3Ga_9$ are quite similar. They are dominated by the main signal at ≈ 6968 eV. This value is by ≈ 10 eV smaller than observed for the standard Eu_2O_3 (electronic configuration $4f^6$, Eu^{3+}) and is characteristic for the $4f^7$ electronic configuration. In both spectra small shoulders are observed on the high-energy side at ≈ 6977 eV indicating the presence of small admixtures of Eu in $4f^6$ configuration. The signature of

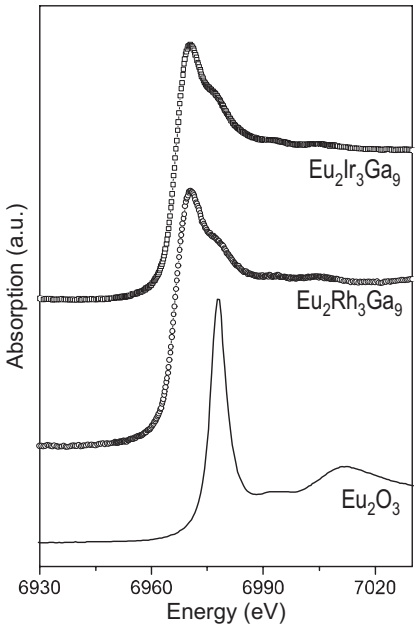

Fig. 7. Eu-L_{III} X-ray absorption spectra of $Eu_2Rh_3Ga_9$ and $Eu_2Ir_3Ga_9$ in comparison with the reference material Eu_2O_3.

both electronic configurations of europium (Eu^{2+} and Eu^{3+}) in the investigated samples of $Eu_2Rh_3Ga_9$ and $Eu_2Ir_3Ga_9$ cannot be explained by impurities. A presence of the two known binary iridium gallides in the $Eu_2Ir_3Ga_9$ samples should not influence the XAS results. Europium in $EuRh_2Ga_8$ as an impurity in the $Eu_2Rh_3Ga_9$ sample also shows clearly the $4f^7$ configuration [30]. The contributions of the $4f^6$ configuration are observed in the X-ray absorption spectra of both compounds. This correlates with the slightly reduced values of effective magnetic moments and may suggest a peculiar bond structure of the $Eu_2T_3Ga_9$ compounds, probably similar to the behaviour of cerium nitride [31, 32].

Conclusion

The ternary phases $Eu_2Rh_3Ga_9$ and $Eu_2Ir_3Ga_9$ complete the respective series $RE_2Rh_3Ga_9$ and $RE_2Ir_3Ga_9$ of the compounds of rare-earth metals and gallium with rhodium or iridium. Caused obviously by covalent interactions between the transition metal and gallium atoms, the *a* and *b* lattice parameters of the orthorhombic crystal structure of the $Y_2Co_3Ga_9$ type are controlled mainly by the puckered layers formed by Rh(Ir) and Ga. The rare-earth metals influence strongly the *c* lattice parameter and thus the unit cell volume. From the behaviour of the unit cell volume of $RE_2T_3Ga_9$ (RE = Y, Sm–Yb, T = Rh, Ir) one can conclude that the europium atoms should not be present in the trivalent state. This was confirmed by measurements of the magnetic susceptibility and the X-ray absorption spectra revealing predominantly the $4f^7$ electronic configuration of europium in both compounds.

Acknowledgements

The authors thank Mrs. M. Eckert and Mrs. S. Müller for microstructure analysis, Mrs. K. Schulze for EDX measurements and Mr. E. Welter for assistance during the XAS experiments (beamline A1 at HASYLAB, DESY, Hamburg). O. Sichevych acknowledges the Max-Planck-Society for a research fellowship.

[1] Yu. N. Grin, R. E. Gladyshevskii, O. M. Sichevych, V. E. Zavodnik, Ya. P. Yarmolyuk, I. V. Rozhdestvenskaya, Sov. Phys. Crystallogr. **29(5)**, 528 (1984).
[2] R. Giedigkeit, W. Schnelle, Yu. Grin, R. Kniep, Collected Abstracts of VIIth European Conference on Solid State Chemistry, Madrid, P 136 (1999).
[3] R. Gladyshevskii, K. Cenzual, H. D. Flack, E. Parthé, Acta Crystallogr. **B49**, 468 (1993).
[4] V. M. T. Thiede, B. Fehrmann, W. Jeitschko, Z. Anorg. Allg. Chem. **625**, 1417 (1999).
[5] G. H. Kwei, A. C. Lawson, A. C. Larson, B. Morosin, E. M. Larson, P. C. Canfield, Acta Crystallogr. **B52**, 580 (1996).
[6] A. Lacerda, P. C. Canfield, W. P. Beyermann, M. F. Hundley, J. D. Thompson, G. Sparn, Z. Fisk, C. Burns, D. Barnhart, A. C. Lawson, G. H. Kwei, J. Goldstone, J. Alloys Compd. **181**, 191 (1992).
[7] J. Niermann, W. Jeitschko, Z. Anorg. Allg. Chem. **630**, 361 (2002).
[8] Ch. Routsi, J. K. Yakinthos, J. Alloys Compd. **323 – 324**, 427 (2001).
[9] S. K. Dhar, C. Mitra, P. Manfrinetti, A. Palenzona, P. Bonville, Physica B **259 – 261**, 150 (1999).
[10] T. Okane, S.-I. Fujimori, A. Ino, A. Fujimori, S. K. Dhar, C. Mitra, P. Manfrinetti, A. Palenzona, O. Sakai, Phys. Rev. B **65**, 125102 (2002).
[11] R. E. Gladyshevskii, K. Cenzual, E. Parthé, J. Alloys Compd. **182**, 165 (1992).
[12] Yu. Grin, P. Rogl, Inorg. Mater. **25(4)**, 593 (1989).
[13] B. Buschinger, C. Geibel, M. Weiden, C. Dietrich, G. Cordier, G. Olesh, J. Köhler, F. Steglich, J. Alloys Compd. **260**, 44 (1997).
[14] B. Buschinger, O. Trovarelli, M. Weiden, C. Geibel, F. Steglich, J. Alloys Compd. **275 – 277**, 633 (1998).

[15] N. O. Moreno, A. Lobos, A. A. Aligia, E. D. Bauer, S. Bobev, V. Fritsch, J. L. Sarrao, P. G. Pagliuso, J. D. Thompson, C. D. Batista, Z. Fisk, Phys. Rev. B **71**, 165107 (2005).
[16] O. Trovarelli, C. Geibel, B. Buschinger, R. Borth, S. Mederle, M. Grosche, G. Sparn, F. Steglich, O. Brosch, L. Donnevert, Phys. Rev. B **60**, 1136 (1999).
[17] J. Niermann, B. Fehrmann, M. W. Wolff, W. Jeitschko, J. Solid State Chem. **177**, 2600 (2004).
[18] A. Hiess, S. Coad, B. Buschinger, O. Trovarelli, J. X. Boucherle, F. Givord, T. Hansen, E. Lelievre-Berna, E. Suard, C. Geibel, F. Steglich, Physica B **259 – 261**, 343 (1999).
[19] R. E. Gladyshevskii, K. Cenzual, E. Parthé, Z. Kristallogr. **203**, 113 (1993).
[20] M. Schlüter, W. Jeitschko, Z. Anorg. Allg. Chem. **626**, 2217 (2000).
[21] R. Rykhal, E. Gladyshevskyii, O. Myakush, A. Fedorchuk, Lviv Polytechnical Institute Visnyk **332**, 7 (1997).
[22] O. Myakush, Ph. D. Thesis, Lviv University (1999).
[23] V. Ya. Markiv, N. N. Belyavina, Kiev University Visnyk, Physics **28,** 17 (1987).
[24] L. G. Akselrud, P. Y. Zavalii, Yu. N. Grin, V. K. Pecharsky, B. Baumgartner, E. Wölfel, Mater. Sci. Forum **133–136**, 335 (1993).
[25] a) X-RED, Version 1.10, STOE Data Reduction Program, STOE & Cie GmbH, Darmstadt (1998); b) X-SHAPE, Version 1.06, Crystal Optimisation for Numerical Absorption Correction, STOE & Cie GmbH, Darmstadt (1999).
[26] L. Akselrud, Yu. Grin, XasWin, Max-Planck-Institut für Chemische Physik fester Stoffe, Dresden (2004).
[27] M. Boström, Yu. Prots, Yu. Grin, Solid State Sci. **6**, 499 (2004).
[28] M. Boström, Yu. Prots, Yu. Grin, J. Solid State Chem. (2006), in press.
[29] L. Pauling, The nature of the chemical bond and the structures of molecules and crystals, Cornell Univ. Press, Ithaca, NY (1960).
[30] O. Sichevych, W. Schnelle, Yu. Prots, U. Burkhardt, M. Schmidt, Yu. Grin, *to be published*.
[31] D. Marterre, C. Brouer, G. Krill, E. Beaurepaire, B. B. Carriére, D. Chandesris, Europhys. Lett. **15**, 687 (1991).
[32] J. P. Kappler, E. Beaurepaire, G. Krill, J. Serenis, C. Godart, G. Olcese, J. Phys. France I **1**, 1381 (1991).